

Deformation performance analysis of thin plates based on a deformation decomposition method

Dongwei Wang^a, Kaixuan Liang^b and Panxu Sun*

School of Civil Engineering, Zhengzhou University, Zhengzhou, 450001, China

(Received January 5, 2022, Revised August 22, 2022, Accepted August 23, 2022)

Abstract. Thin plates are the most common spatially stressed members in engineering structures that bear out-of-plane loads. Therefore, it is of great significance to study the deformation performance characteristics of thin plates for structural design. By constructing 12 basic displacement and deformation basis vectors of the four-node square thin plate element, a deformation decomposition method based on the complete orthogonal mechanical basis matrix is proposed in this paper. Based on the deformation decomposition method, the deformation properties of the thin plate can be quantitatively analyzed, and the areas dominated by each basic deformation can be visualized. In addition, the method can not only obtain more deformation information of the structure, but also identify macroscopic basic deformations, such as bending, shear and warping deformations. Finally, the deformation properties of the bidirectional thin plates with different sizes of central holes are analyzed, and the changing rules are obtained.

Keywords: central hole; complete orthogonality; deformation decomposition; thin plate; warping deformation

1. Introduction

Thin plate is a common structural component, widely used in civil engineering, machinery, composite materials and other fields (Wang *et al.* 2018, Li *et al.* 2020, Dehghani *et al.* 2021). Compared with beams, columns and other components, thin plate structures are prone to out-of-plane deformation under the influence of external loads, temperature, humidity, uneven materials, residual stress, and other factors (Lederle and Hiller 2012, Ren and Wang 2019, Xu *et al.* 2017, Zhu *et al.* 2020). Plate is a kind of spatial component with more complex mechanical properties. Out-of-plane deformation of plates is often accompanied by the warping phenomenon. The warping deformation is an important out-of-plane deformation, which is of great significance to the study of plate problems (Taylor 1933, Loredo 2016, Polizzotto 2018). Compared with conventional plane deformations (tensile, compression, shear, etc.), the spatial warping deformation is more complex and has an impact on the mechanical properties of the plate (Kordolemis and Weaver 2017), which brings more difficulties to the analysis and design of the plate structure. Although not the main deformation, the proportion of warping deformation cannot be ignored (especially at the corners of the plate). Especially in engineering, it is a common measure to set additional

reinforcement at the corners of the plate to prevent cracking (ACI 2011).

In practical engineering, due to the needs of use, it is often necessary to form holes of different sizes on the thin plate. Compared with the thin plate without opening, the deformation performance of the thin plate with a hole is more complicated. In most cases, the presence of the hole only produces stress changes on a local area around the hole (Wang and Spencer 2021). However, the appearance of the hole will also change the original force transmission mechanism of the plate structure, thereby affecting its deformation performance (Kalaycioglu *et al.* 2019). At the same time, the hole impairs the ability of the plate to resist warping deformation, resulting in a sudden increase in stress concentration near the hole and warping deformation (Jafari and Ardalani 2016, Tuna and Trovalusci 2020), which eventually leads to cracking of the plate (Yan 2006). Therefore, it is an important subject to study the out-of-plane warping deformation properties of thin plates (especially the thin plate with a hole).

As a powerful numerical method, finite element analysis has become the focus of researchers and engineers. Many scholars have developed plate elements that can account for the warping deformation (Piltner 1992, Katili *et al.* 2015, Shang *et al.* 2016), and then identify warping deformation based on the nodal displacements of the thin plate model. However, the deformation obtained by the nodal displacement cloud map is actually a comprehensive out-of-plane deformation, which consists of deformations such as warping, torsion, and bending (Piana *et al.* 2021). In engineering, it is usually necessary to implement different reinforcement measures for different deformations (Hwang *et al.* 2019, Saliba and Gardner 2018). Although reinforcement at large deformation locations can reduce various deformations including warping, this method is not

*Corresponding author, Ph.D.

E-mail: panxusun@zzu.edu.cn

^aProfessor

E-mail: dongweiwang@zzu.edu.cn

^bPh.D. Student

E-mail: 202011211030241@gs.zzu.edu.cn

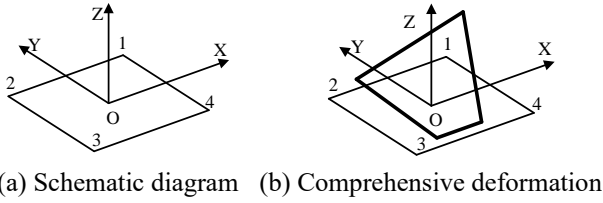


Fig. 1 Four-node square thin plate element

economical and sometimes it is difficult to achieve the desired effect. Therefore, it is necessary to decompose the comprehensive deformation of the thin plate into basic deformations to achieve the purpose of guiding targeted reinforcement. However, the solution object of traditional finite element strain analysis is the strain of each element, and it is difficult to obtain complete basic deformation information and effectively distinguish warping deformation from comprehensive deformation.

As a powerful statistical tool, Proper Orthogonal Decomposition (POD) is widely used in fluid mechanics, image recognition, optimal control and other fields (Tang *et al.* 2015, Janiga 2019, Ali *et al.* 2021). The basic principle of the POD method is to obtain several linearly independent orthonormal bases by processing the physical field data obtained by numerical simulation or experiment. By representing the physical field under arbitrary design parameters as a linear combination of orthonormal bases and its corresponding coefficients, dimensionality reduction and decoupling of the physical field can be achieved. Therefore, POD can be applied to decompose the comprehensive deformation represented by the nodal displacement field. However, for displacement fields with a large number of meshes, it is difficult for traditional POD methods to solve the orthonormal basis. Even if an auxiliary algorithm (Girfoglio *et al.* 2021) is used in the solution, there is no guarantee that the obtained basis matrix conforms to the characteristics of the basic deformation.

Therefore, on the basis of satisfying mathematical orthogonality and mechanical equilibrium, a deformation decomposition method of the four-node square thin plate element is proposed and applied to the deformation analysis of thin plate structures. By quantitatively identifying the basic deformation of the four-side-fixed thin plate under a uniformly distributed load, the deformation decomposition diagram and the warping deformation proportion cloud diagram are obtained. The correctness of the method is verified by comparing the results with the traditional finite element strain analysis. Then on this basis, the deformation properties of the bidirectional thin plates with different sizes of central holes are analyzed.

2. Deformation decomposition method based on orthogonal theory

2.1 The construction of complete orthogonal mechanical bases

The schematic diagram of the four-node square thin plate element is shown in Fig. 1. Based on the linear finite

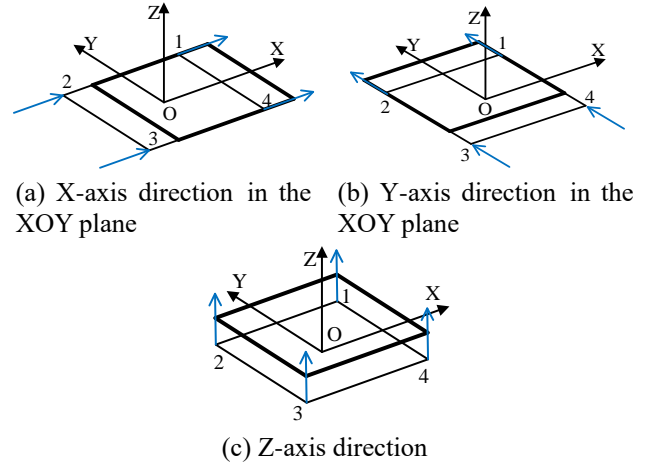


Fig. 2 Rigid body linear displacements

element theory, under the assumption of small deformation, the comprehensive deformation of the element can be represented by 12 nodal linear displacements of the 4 nodes of the element, and the deformation space formed by 12 nodal linear displacements can be linearly represented by 12 completely orthogonal basic rigid body displacement or elastic deformation basis vectors (Hassani 2013).

The basic displacements of the four-node square thin plate element include the displacement of the rigid body in the X-, Y-, and Z-axis directions and the rotation of the rigid body in the XOY, YOZ, and XOZ planes. The basic deformations of the element include tensile and compressive deformations in the X- and Y-axis directions of the XOY plane, bending deformation in the X- and Y-axis directions of the XOY plane, shear deformation in the XOY plane, and warping deformation in the Z-axis direction.

On the four nodes of the four-node square thin plate element, loads of equal magnitude and the same direction are applied along the X- and Y-axis directions, respectively, resulting in rigid body linear displacements in the X-, Y-, and Z-axis directions, as shown in Fig. 2. Then, for the rigid body linear displacement in the X-, Y-, and Z- axis directions, the construction of three basis vector is performed.

Basis vector of rigid body linear displacement in the X-axis direction of the XOY plane (as shown in Fig. 2(a)) is

$$P_1 = \begin{pmatrix} 0.5000 & 0 & 0 & 0.5000 & 0 & 0 \\ 0.5000 & 0 & 0 & 0.5000 & 0 & 0 \end{pmatrix}^T \quad (1)$$

Basis vector of rigid body linear displacement in the Y-axis direction of the XOY plane (as shown in Fig. 2(b)) is

$$P_2 = \begin{pmatrix} 0 & 0.5000 & 0 & 0 & 0.5000 & 0 \\ 0 & 0.5000 & 0 & 0 & 0.5000 & 0 \end{pmatrix}^T \quad (2)$$

Basis vector of rigid body linear displacement in the Z-axis (as shown in Fig. 2(c)) is

$$P_3 = \begin{pmatrix} 0 & 0 & 0.5000 & 0 & 0 & 0.5000 \\ 0 & 0 & 0.5000 & 0 & 0 & 0.5000 \end{pmatrix}^T \quad (3)$$

On the four nodes of the four-node square thin plate

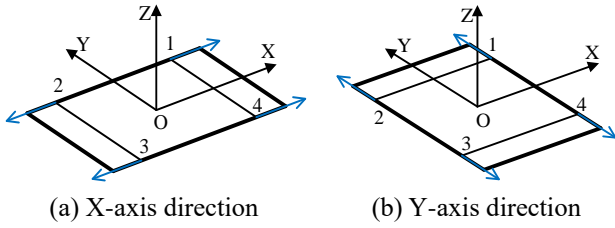


Fig. 3 Tensile and compressive deformations in the XOY plane

element, loads of equal magnitude and opposite directions are applied along the X- and Y-axis directions, respectively, resulting in tensile and compressive deformations in the X- and Y-axis directions, as shown in Fig. 3. At this time, the force condition satisfies both the force balance condition and the moment balance condition.

The basis vector of tensile and compressive deformation in the X-axis direction of the XOY plane is constructed (as shown in Fig. 3(a)) as

$$\mathbf{P}_4 = \begin{pmatrix} 0.5000 & 0 & 0 & -0.5000 & 0 & 0 \\ -0.5000 & 0 & 0 & 0.5000 & 0 & 0 \end{pmatrix}^T \quad (4)$$

Similarly, the basis vector of tensile and compressive deformation in the Y-axis direction of the XOY plane is constructed (as shown in Fig. 3(b)) as

$$\mathbf{P}_5 = \begin{pmatrix} 0 & 0.5000 & 0 & 0 & 0.5000 & 0 \\ 0 & -0.5000 & 0 & 0 & -0.5000 & 0 \end{pmatrix}^T \quad (5)$$

Between the basis vectors of tension-compression deformation, and between the basis vector of tension-compression deformation and the basis vector of rigid body linear displacement, the orthogonal and normalization conditions are satisfied.

According to the established force system balance and moment balance conditions, the basis vectors of other basic deformations and rotations can be constructed. These basis vectors, as well as the basis vectors of the above-mentioned rigid body linear displacement and tension-compression deformation, satisfy mutual orthogonalization and normalization conditions. The corresponding force conditions, deformations or rotations are shown in Fig. 4.

Basis vector of bending deformation in the X-axis direction of the XOY plane (as shown in Fig. 4(a)) is

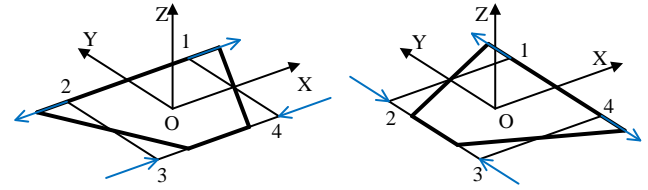
$$\mathbf{P}_6 = \begin{pmatrix} 0.5000 & 0 & 0 & -0.5000 & 0 & 0 \\ 0.5000 & 0 & 0 & -0.5000 & 0 & 0 \end{pmatrix}^T \quad (6)$$

Basis vector of bending deformation in the Y-axis direction of the XOY plane (as shown in Fig. 4(b)) is

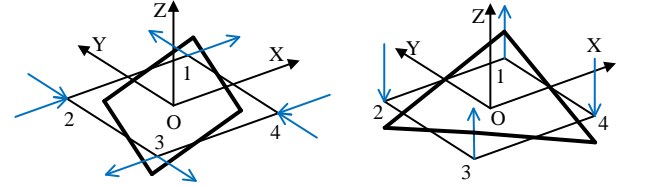
$$\mathbf{P}_7 = \begin{pmatrix} 0 & 0.5000 & 0 & 0 & -0.5000 & 0 \\ 0 & 0.5000 & 0 & 0 & -0.5000 & 0 \end{pmatrix}^T \quad (7)$$

Basis vector of shear deformation in the XOY plane (as shown in Fig. 4(c)) is

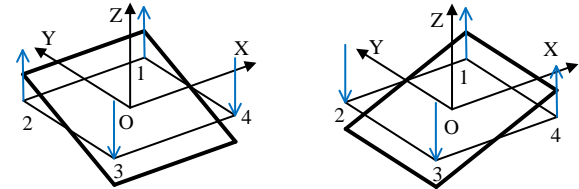
$$\mathbf{P}_8 = \begin{pmatrix} 0.3536 & 0.3536 & 0 & 0.3536 \\ -0.3536 & 0 & -0.3536 & -0.3536 \\ 0 & -0.3536 & 0.3536 & 0 \end{pmatrix}^T \quad (8)$$



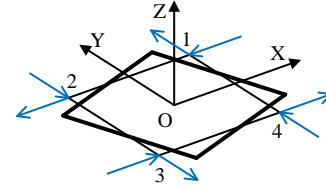
(a) Bending deformation in the X-axis direction of the XOY plane (b) Bending deformation in the Y-axis direction of the XOY plane



(c) Shear deformation in the XOY plane (d) Warping deformation in the Z-axis direction



(e) Rigid body rotation in the YOZ plane (f) Rigid body rotation in the XOZ plane



(g) Rigid body rotation in the XOY plane

Fig. 4 Other 4 basic deformations and 3 rotational displacements of the four-node square thin plate element

Basis vector of warping deformation in the Z-axis direction (as shown in Fig. 4(d)) is

$$\mathbf{P}_9 = \begin{pmatrix} 0 & 0 & 0.5000 & 0 & 0 & -0.5000 \\ 0 & 0 & 0.5000 & 0 & 0 & -0.5000 \end{pmatrix}^T \quad (9)$$

Basis vector of rigid body rotational displacement in the YOZ plane (as shown in Fig. 4(e)) is

$$\mathbf{P}_{10} = \begin{pmatrix} 0 & 0 & 0.5000 & 0 & 0 & 0.5000 \\ 0 & 0 & -0.5000 & 0 & 0 & -0.5000 \end{pmatrix}^T \quad (10)$$

Basis vector of rigid body rotational displacement in the XOZ plane (as shown in Fig. 4(f)) is

$$\mathbf{P}_{11} = \begin{pmatrix} 0 & 0 & 0.5000 & 0 & 0 & -0.5000 \\ 0 & 0 & -0.5000 & 0 & 0 & 0.5000 \end{pmatrix}^T \quad (11)$$

Basis vector of rigid body rotational displacement in the XOY plane (as shown in Fig. 4(g)) is

$$\mathbf{P}_{12} = \begin{pmatrix} -0.3536 & 0.3536 & 0 & -0.3536 \\ -0.3536 & 0 & 0.3536 & -0.3536 \\ 0 & 0.3536 & 0.3536 & 0 \end{pmatrix}^T \quad (12)$$

Table 1 Colours corresponding to basic deformations

Tensile deformation in the X-axis direction (T-X)	Compressive deformation in the X-axis direction (C-X)	Tensile deformation in the Y-axis direction (T-Y)	Compressive deformation in the Y-axis direction (C-Y)
Bending deformation in the X-axis direction (B-X)	Bending deformation in the Y-axis direction (B-Y)	Shear deformation (S)	Warping deformation (W)

The constructed 12 basis vectors satisfy the orthogonal and normalization conditions with each other, namely

$$P_i^T P_j = \begin{cases} 1 & i = j \\ 0 & i \neq j \end{cases} \quad (i, j = 1, 2, \dots, 12) \quad (13)$$

Based on the theoretical basis of orthogonal decomposition, the complete orthogonal mechanical basis matrix of the four-node square thin plate element is obtained as

$$P = [P_1 \ P_2 \ P_3 \ P_4 \ P_5 \ P_6 \ \dots \ P_{11} \ P_{12}] \quad (14)$$

The 12×12 basis matrix **P** satisfies completeness and **P**·**P**^T=**E**, which can be used as the complete orthogonal mechanical basis matrix for deformation decomposition. **E** is the identity matrix.

2.2 Deformation decomposition method based on the complete orthogonal mechanical basis matrix

The nodal displacement vector of any comprehensive deformation of the four-node square thin plate element is

$$d_e = (\begin{matrix} x_1' - x_1 & y_1' - y_1 & z_1' - z_1 & x_2' - x_2 \\ y_2' - y_2 & z_2' - z_2 & x_3' - x_3 & y_3' - y_3 \\ z_3' - z_3 & x_4' - x_4 & y_4' - y_4 & z_4' - z_4 \end{matrix})^T \quad (15)$$

The nodal displacement vector of the four-node square thin plate element can be projected onto the constructed complete orthogonal basis matrix **P**.

$$d_e = p \cdot P^T \quad (16)$$

where

$$p = (\begin{matrix} p_1 & p_2 & p_3 & p_4 & p_5 & p_6 \\ p_7 & p_8 & p_9 & p_{10} & p_{11} & p_{12} \end{matrix}) \quad (17)$$

where *p_i* represents the projection coefficient on the corresponding basic displacement or basic deformation basis vector.

Eq. (16) can be converted to

$$p = d_e \cdot P \quad (18)$$

The positive or negative of projection coefficients can represent the actual state of rigid body displacement or basic deformation. For *p₄* and *p₅*, a positive value means the element is in tension, and a negative value means the element is in compression. Accordingly, the arbitrary comprehensive deformation of the element described by the element node displacement can be decomposed into orthogonal components such as rigid body linear displacement, basic deformation, and rigid body rotation.

Furthermore, the separation of the rigid and flexible components of the element rigid body linear displacements, basic deformations and rigid body rotational displacements can be carried out for Eq. (19).

$$p = (p^L \ p^D \ p^R) \quad (19)$$

where **p^L**=(*p₁* *p₂* *p₃*) is the projection coefficient vector of the rigid body linear displacements, **p^R**=(*p₄* *p₅* *p₆* *p₇* *p₈* *p₉*) is the projection coefficient vector of the basic deformations, **p^D**=(*p₁₀* *p₁₁* *p₁₂*) is the projection coefficient vector of the rigid body rotational displacements.

If **pⁱ** = $\frac{|p_i|}{\sum_{i=4}^9 |p_i|}$, the projection coefficients of the basic deformations can be normalized.

$$p^D = (p_4' \ p_5' \ p_6' \ p_7' \ p_8' \ p_9') \quad (20)$$

where *p_i'* (*i* = 4, 5, ..., 9) represents the proportion of each basic deformation in the total basic deformation.

Ignoring the effect of rigid body displacements, the absolute values of the projection coefficients on the six basic deformation basis vectors are compared. The basis corresponding to the projection coefficient with the largest absolute value represents the main basic deformation form of the element. For ease of analysis, each basic deformation corresponds to a colour and an abbreviation, and the tensile and compressive deformations are separated. The colour and abbreviation descriptions are shown in Table 1. Red represents that the element is dominated by X-axis compressive deformation (C-X), and blue represents that the element is dominated by shear deformation (S).

2.3 Error analysis

Rigid body rotational displacement is a nonlinear displacement, and its linear decomposition will produce errors, that is, the rigid body rotational displacement vector of the element will not only be projected onto the rigid body rotational displacement basis vector, but also onto other rigid body linear displacement and basic deformation basis vectors. Therefore, it is necessary to calculate the additional projection coefficients produced by the rigid body rotational displacement of the element on other rigid body linear displacement and basic deformation basis vectors, and analyse whether they affect the calculation accuracy.

When the four-node square thin plate element with side length *l* rotates clockwise around the centre (i.e., the coordinate origin) in the plane, the displacement vector of its four nodes is

$$d_e = \left(\frac{\sqrt{2}l}{2} \sin(\frac{\pi}{4} - \theta) - \frac{l}{2} \quad \frac{\sqrt{2}l}{2} \cos(\frac{\pi}{4} - \theta) - \frac{l}{2} \quad 0 \right)$$

$$\begin{pmatrix} \frac{l}{2} - \frac{\sqrt{2}l}{2} \cos(\frac{\pi}{4} - \theta) & \frac{\sqrt{2}l}{2} \sin(\frac{\pi}{4} - \theta) - \frac{l}{2} & 0 \\ \frac{l}{2} - \frac{\sqrt{2}l}{2} \sin(\frac{\pi}{4} - \theta) & \frac{l}{2} - \frac{\sqrt{2}l}{2} \cos(\frac{\pi}{4} - \theta) & 0 \\ \frac{\sqrt{2}l}{2} \cos(\frac{\pi}{4} - \theta) - \frac{l}{2} & \frac{l}{2} - \frac{\sqrt{2}l}{2} \sin(\frac{\pi}{4} - \theta) & 0 \end{pmatrix} \quad (21)$$

The rigid body rotational displacement vector of the element is projected onto the constructed complete orthogonal mechanical basis matrix. The rigid body rotational displacement vector of the element has projection coefficients only on the rigid body rotational displacement basis vector, X-axis tensile-compressive deformation basis vector, and Y-axis tensile-compressive deformation basis vector. All other rigid body linear displacement and basic deformation basis vectors have projection coefficients of 0. Therefore, the equation system of the projection coefficient corresponding to the rigid body rotational displacement vector can be obtained as

$$\begin{cases} 0.5p_4 + 0p_5 + 0.3536p_{12} = \frac{\sqrt{2}l}{2} \sin(\frac{\pi}{4} - \theta) - \frac{l}{2} \\ 0p_4 + 0.5p_5 - 0.3536p_{12} = \frac{\sqrt{2}l}{2} \cos(\frac{\pi}{4} - \theta) - \frac{l}{2} \\ -0.5p_4 + 0p_5 + 0.3536p_{12} = \frac{l}{2} - \frac{\sqrt{2}l}{2} \cos(\frac{\pi}{4} - \theta) \end{cases} \quad (22)$$

where p_4 is the projection coefficient of the basis vector of tensile and compressive deformation in the X-axis direction of the XOY plane, p_5 the projection coefficient of the basis vector of tensile and compressive deformation in the Y-axis direction of the XOY plane, p_{12} is the projection coefficient of the basis vector of rigid body rotational displacement in the XOY plane.

Solving Eq. (22), we can get

$$\begin{cases} p_4 = p_5 = l(\cos \theta - 1) \\ p_{12} = -\sqrt{2}l \sin \theta \end{cases} \quad (23)$$

Taylor series expansion is taken for $\sin \theta$ and $\cos \theta$ in Eq. (23). Ignoring the higher-order small quantity, we can get

$$\begin{cases} p_4 = p_5 \approx l(1 - \frac{\theta^2}{2} - 1) = -\frac{l\theta^2}{2} \\ p_{12} = -\sqrt{2}l\theta \\ \left| \frac{p_4}{p_{12}} \right| = \left| \frac{p_5}{p_{12}} \right| = \frac{\theta}{2\sqrt{2}} \end{cases} \quad (24)$$

From Eq. (24), in the case of small deformations, p_4 and p_5 are higher-order small quantities with respect to p_{12} , considering their relation to θ . Therefore, p_4 and p_5 can be ignored, and the error is acceptable. The rigid body rotational displacement vector can be approximated simply by projecting onto the basis vector of the rigid body rotational displacement in the XOY plane.

3. Warping deformation analysis of bidirectional thin plates with four-side-fixed support

According to the theory of elasticity, the vertical normal strain and vertical shear strain can be ignored in the strain analysis of thin plates (Landau and Lifshitz 2009).

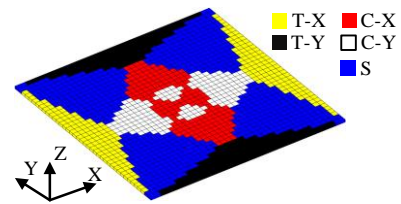


Fig. 5 Deformation decomposition diagram of model A1

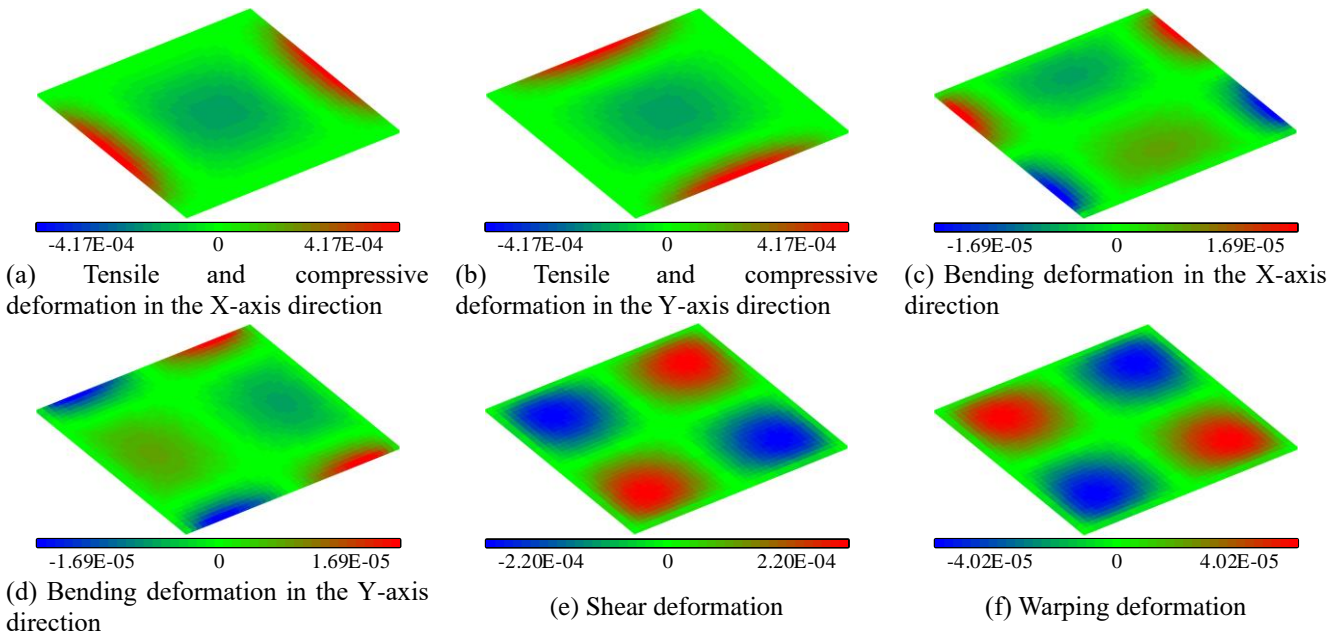


Fig. 6 Deformation cloud diagram of model A1

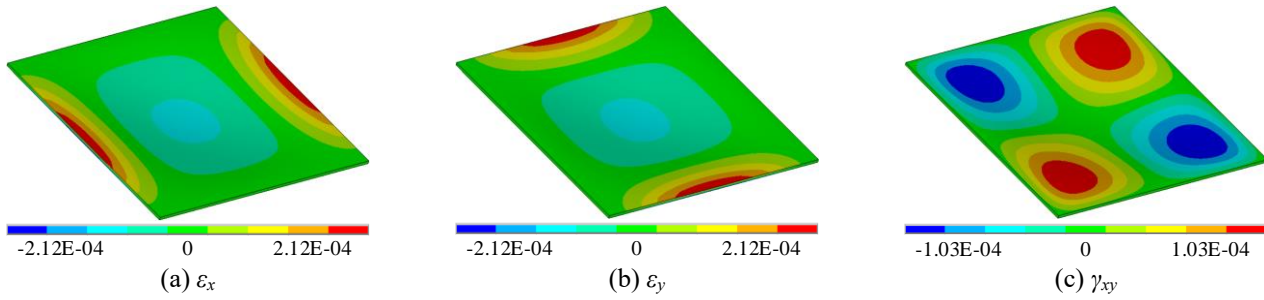


Fig. 7 Strain cloud diagram of model A1

Table 2 The size parameters and material properties of models B1, B2 and C

Model	Size /mm	Elastic modulus /MPa	Density /kg/m ³	Number of elements
B1	100×130×500	2.1×10 ⁵	7850	20×26×100
B2	100×130×500	2.1×10 ⁵	7850	20×26×100
C	100×100×1	2.1×10 ⁵	7850	20×20

Therefore, in the finite element analysis of thin plates, the 3D cube element can be simplified to a four-node square thin plate element. Furthermore, the four-node square thin plate element can be used to divide the thin plate and decompose its deformation. For all the thin plate models in this study, the length and width directions are set as the X and Y axes, respectively, and the thickness direction is the Z axis.

3.1 Finite element verification of the deformation decomposition method

Taking the thin plate A1 fixed on four sides as an example, its length and width are both 400 mm. The thickness is 5 mm. The elastic modulus E is 2.1×10^5 MPa. The density $\rho = 7850$ kg/m³, and the Poisson's ratio $\mu = 0.3$. A1 is subjected to a uniformly distributed load of 4 kN/m² perpendicular to the plate surface. The finite element model of A1 is established with SHELL181 elements, and the number of elements used in both the X- and Y- axis directions is 40. The deformation decomposition diagram of A1 can be obtained using the method mentioned in Section 1, as shown in Fig. 5. According to the magnitude of the projection coefficient, the cloud diagram of specific deformation can be drawn, as shown in Fig. 6.

Since the ratio of the plate thickness to the minimum characteristic length of the plate surface is 1/80, according to thin plate theory, secondary strains such as ε_z , γ_{xz} and γ_{yz} can be ignored. It is only necessary to analyse the effect of the main strains ε_x , ε_y and γ_{xy} on the plate (Landau and Lifshitz 2009). The strain cloud diagram is shown in Fig. 7.

Comparing Fig. 5 to Fig. 7, it can be seen that there are large normal strains ε_x in the centre, and left and right boundary areas of model A1, mainly manifested as tensile and compressive deformations in the X-axis direction (corresponding to the red and yellow areas in Fig. 5). The normal strain ε_y in the centre, and upper and lower boundary areas of model A1 is also large, mainly manifested as tensile and compressive deformations in the Y-axis direction (corresponding to the black and white areas in Fig. 5). At the four corners of model A1, the shear strain

γ_{xy} of the XOY plane is large, which is mainly manifested as the shear deformation of the XOY plane (corresponding to the blue area in Fig. 5). In addition, the deformation cloud diagram and the strain cloud diagram also have a good correspondence (i.e., Figs. 6(a), 6(b) and 6(e) correspond to Figs. 7(a), 7(b) and 7(c), respectively).

Hence, the deformation decomposition results of model A1 are consistent with the finite element strain analysis results, which verifies the correctness of the deformation decomposition method based on orthogonal theory. More importantly, the finite element strain analysis can only identify the normal strain and shear strain of the structure, while the deformation decomposition method can further obtain the macroscopic bending and warping deformation of the element on the basis of identifying the tensile, compressive and shear deformations.

3.2 Verification of the warping deformation basis vector

According to the theory of material mechanics, the cross-section of a circular rod of equal cross-section remains flat after torsion. However, the outer circumference of a rod with non-circular (square, rectangle, triangle, oval, etc.) cross-section no longer in the same plane as its original shape, resulting in warping (Gere and Timoshenko 1997).

The thin plate element adopts SHELL181, which has only 4 nodes and cannot be exerted spatial torque. Hence, in order to analyse the out-of-plane deformation of the thin plate under torsional conditions, two solid element models B1 and B2 with rectangular equal-sections are established with eight-node SOLID45 elements, and thin plate C is established with four-node SHELL181 elements. The dimensional parameters and material properties of models B1, B2 and C are shown in Table 2. Then, models B1, B2 and C are combined into a whole by applying binding contact constraint on them, as shown in Fig. 8. Equal and opposite torques of 2.3 kN/m are applied to the ends of models B1 and B2, respectively.

Under the action of torques at both ends, the nodal displacement cloud diagrams of the Z-axis direction of

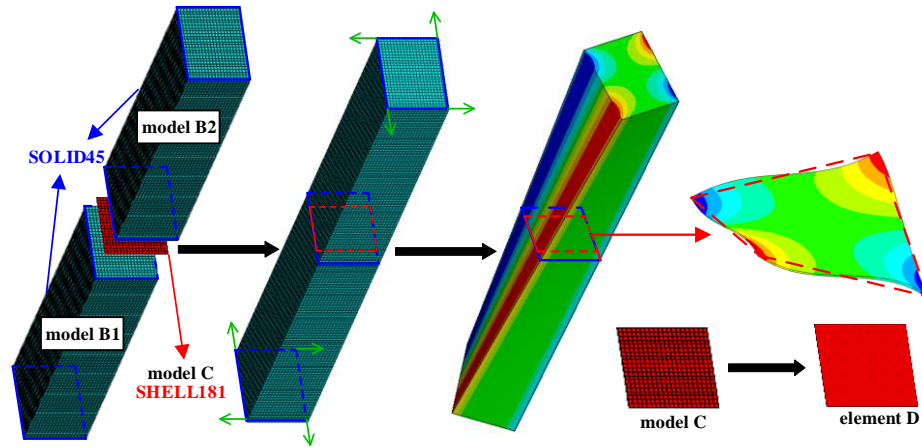


Fig. 8 Schematic diagram of warping deformation of thin plate under torsion condition

Table 3 The proportion of each basic deformation of element D

p_4'	p_5'	p_6'
0	0	0
p_7'	p_8'	p_9'
0	0	100%

models B1, B2 and C can be obtained by using finite element software ANSYS, as shown in Fig. 8. In order to eliminate the effect of stress concentration, only the deformation of model C is analysed according to Saint Venant's principle. For the convenience of analysis, the deformation scale factor of model C is enlarged to make the deformation more obvious. The entire model C is regarded as a large four-node square thin plate element and named element D, whose nodal displacement vector d_e is

$$d_e = \begin{pmatrix} 1.18 & -1.18 & 1.15 & 1.18 \\ 1.18 & -1.15 & -1.18 & 1.18 \\ 1.15 & -1.18 & -1.18 & -1.15 \end{pmatrix} \times 10^{-5} \quad (25)$$

Deformation decomposition of element D is carried out, and the rigid body displacements are ignored. The proportion of each basic deformation are shown in Table 3.

It can be seen from Table 3 that under the action of torque, the deformation of the thin plate in the middle of the span of the rectangular rod with equal cross-section is decomposed, and only the warping deformation can be obtained. This result is consistent with the material mechanics theory, which verifies the correctness of the warping deformation basis vector of the four-node square thin plate element.

3.3 Analysis of warping deformation of the thin plate

Based on the correctness of the warping deformation basis vector of the four-node square thin plate element, the warping deformation is analysed separately. The proportion of warping deformation of each element to the total deformation of model A1 is extracted, and the warping deformation proportion cloud diagram can be obtained, as shown in Fig. 9.

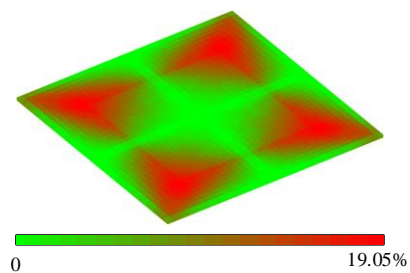


Fig. 9 Warping deformation proportion cloud diagram of model A1

Table 4 Warping deformation analysis results of models A1 to A4

Model	A1	A2	A3	A4
Thickness-to-span ratio	1:80	1:100	1:150	1:250
W_m	19.05%	19.18%	18.76%	19.04%
W_a	6.38%	6.38%	6.38%	6.38%

It can be seen from Fig. 9 that the warping deformation in model A1 accounts for a large proportion at the corners of the thin plate, and its maximum value reaches 19.05%, which cannot be ignored. Hence, by changing the side length of model A1, thin plate models with thickness-span ratios of 1:100, 1:150 and 1:200 are constructed, named A2 to A4. Models A2 to A4 use the same number of elements in each direction as model A1. Under a vertical uniformly distributed load of 4 kN/m², the maximum value W_m and average value W_a of the warping deformation proportion in all elements of A1 to A4 are extracted, and the results are shown in Table 4.

It can be seen from Table 4 that as the thickness-to-span ratio of the thin plate decreases, the maximum value of the warping deformation proportion in the total deformation of the element remains almost unchanged, which is about 19.0%. The average is about 6.4%. For thin plates with different thickness-to-span ratios, the areas with large warping deformation occurs at the four corners of the plate, and the warping deformation at the centre and the four boundaries of the plate accounts for a small proportion of the total deformation of the element, even 0. Therefore, for thin plates, the warping deformation cannot be ignored.

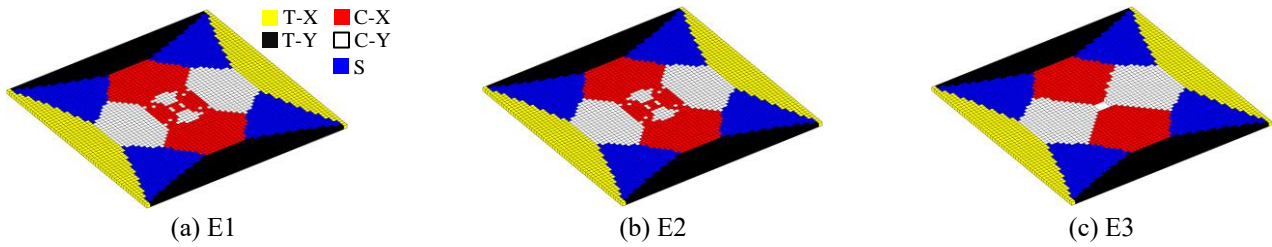


Fig. 10 Deformation decomposition diagrams of models E1 to E3

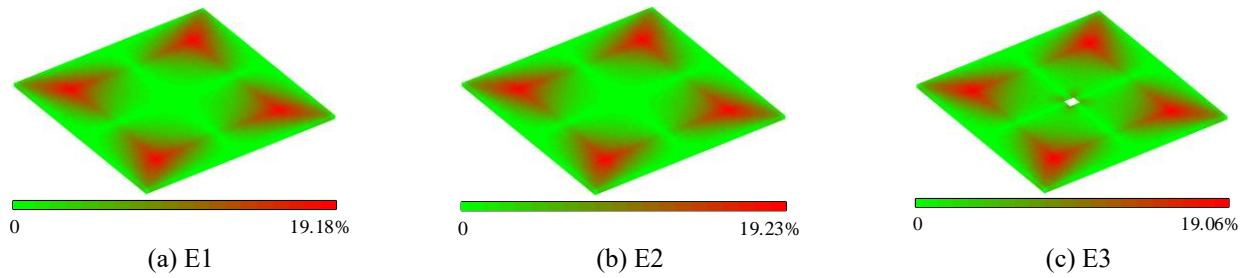
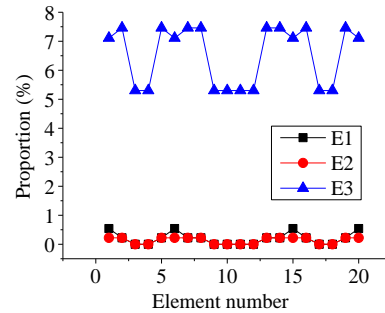


Fig. 11 Warping deformation proportion cloud diagrams of models E1 to E3

15	16	17	18	19	20
13					14
11					12
9					10
7					8
1	2	3	4	5	6



(a) Number of elements around the H-area (b) Proportion of warping deformation of elements
 Fig. 12 Proportion of warping deformation of elements around the H-area in models E1 to E3

4. Performance analysis of bidirectional thin plates with a hole in the centre supported on four sides

The size of the hole has a significant impact on the performance of the thin plate (Jafari and Ardalani 2016). In this section, the deformation decomposition method is used to analyse the deformation performance of the bidirectional thin plate with a square hole in the centre. Taking a square thin plate with a square hole in the centre under the action of uniformly distributed load as an example, the influence of holes of different sizes on its deformation performance is studied. All thin plates in this section are established using SHELL181 elements.

4.1 Effect of a small hole on the performance of the thin plate

The length and width of the thin plate E1 are both 300 mm, and the thickness is 5 mm. The 20 mm×20 mm area in the centre of the plate is called the H-area, and the rest is the P-area. A distributed load of 4 kN/m² perpendicular to the plate surface is applied to the H- and P-areas of E1. For model E2, the model parameters, load magnitude and direction are the same as those of E1, except that the load acts only on the P-area. For model E3, a hole is made in the

H-area of E1, while other parameters remain unchanged. The finite element models of E1 to E3 are established with SHELL181 elements, and the number of elements used in both the X- and Y- axis directions is 60. Models E1 to E3 are decomposed to obtain their deformation decomposition diagrams and warping deformation proportion cloud diagrams under uniformly distributed load, as shown in Figs. 10 to 11.

It can be seen from Fig. 10 that the deformation decomposition diagrams of E1 and E2 are the same, indicating that unloading in the H-area does not affect the main deformation properties of the thin plate. Moreover, after the introduction of the central hole, there is no shear deformation around the hole of E3, that is, when the ratio of the side length of the hole to the side length of the plate is 1:15, there is no need to improve the shear resistance design around the hole. However, as can be seen by comparing Figs. 10(a) and 10(c), the presence of the hole increases the warping deformation of the thin plate in its vicinity.

A comparative analysis of the warping deformation around the H-area of E1 to E3 is conducted. The location and number of elements are shown in Fig. 12(a), and the warping deformation proportion of each element is shown in Fig. 12(b).

It can be seen from Figs. 11(a) to 11(c) and Fig. 12(b)

Table 5 Dimensional parameters of models E4 to E6

Serial number	Side length of plate/mm	Thickness/mm	Thickness-to-span ratio	Side length of hole /mm	Ratio of hole side length to plate side length	Number of elements used in two directions
E4	400	5	1:80	30	1:13.33	80×80
E5	350	5	1:70	30	1:11.67	70×70
E6	300	5	1:60	30	1:10	60×60

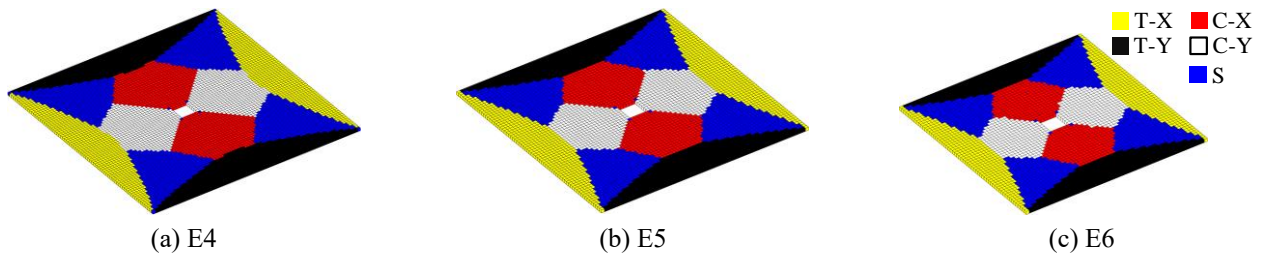


Fig. 13 Deformation decomposition diagrams of models E4 to E6

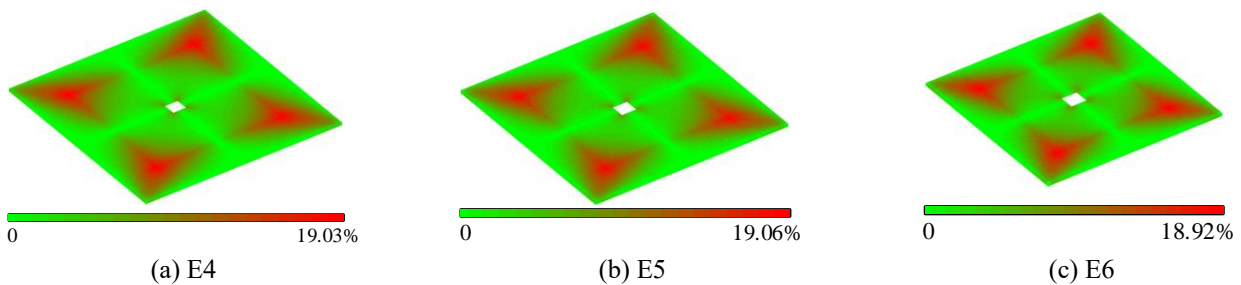


Fig. 14 Warping deformation proportion cloud diagrams of models E4 to E6

Table 6 Dimensional parameters of models E7 to E9

Serial number	Side length of plate/mm	Thickness /mm	Thickness-to-span ratio	Side length of hole /mm	Ratio of hole side length to plate side length	Number of elements used in two directions
E7	240	5	1:48	40	1:6	48×48
E8	360	5	1:72	60	1:6	72×72
E9	480	5	1:96	80	1:6	96×96

that the warping deformation proportion cloud diagram of model E2 has little change compared with model E1, and the warping deformation proportions of the elements near the H-area are very similar, indicating that unloading of the H-area does not affect the warping deformation of the thin plate, while opening a hole leads to obvious warping deformation in the area near the hole of the plate, especially at the corners. Therefore, when a small hole is set in the centre of the thin plate, there is no need for shear deformation resistance design around the hole. However, it is necessary to carry out the warping deformation resistance design, and the corners of the hole should be given priority.

Taking the thin plates E4 to E6 with hole as examples, the size parameters are presented in Table 5. E4 to E6 have the same material properties as A1 and subjected to a distributed load of 4 kN/m². The decomposition results of E4 to E6 are shown in Figs. 13 and 14.

By comparing Fig. 10(c) and Fig. 13, it can be seen that when the side length of the hole increases from 20 mm to 30 mm, the areas dominated by shear deformation (blue areas) begin to appear at the corners of the central hole. Combining with Figs. 13 and 14, as the side length of the hole to the side length of the plate increases, the warping

deformation resistance design should also be carried out with the shear deformation resistance design.

4.2 Effect of a large hole on the performance of the thin plate

This section continues to increase the side length of the hole and maintain the ratio of the side length of the hole to the side length of the plate at 1:6, thereby constructing the thin plate models E7-E9. The size parameters are presented in Table 6. The deformation decomposition results are shown in Figs. 15 to 16.

By comparing Fig. 13 and Fig. 15, it can be seen that when the ratio of the side length of the hole to the side length of the plate is 1:6, the main area of shear deformation at the corner of the hole and the main area of shear deformation at the corner of the thin plate begin to be connected. Therefore, when the ratio of the side length of the hole to the side length of the plate is greater than 1:6, a shear deformation resistance design should be added along the connection lines between the corner of the hole and the corner of the plate. In addition, Fig. 16 shows that warping deformation resistance design should be added to the

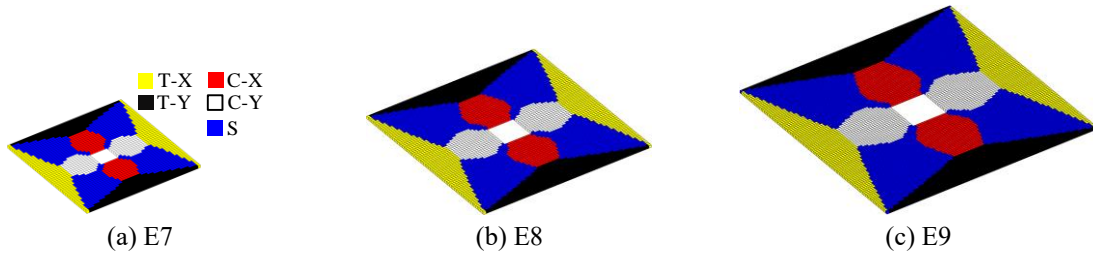


Fig. 15 Deformation decomposition diagrams of models E7 to E9

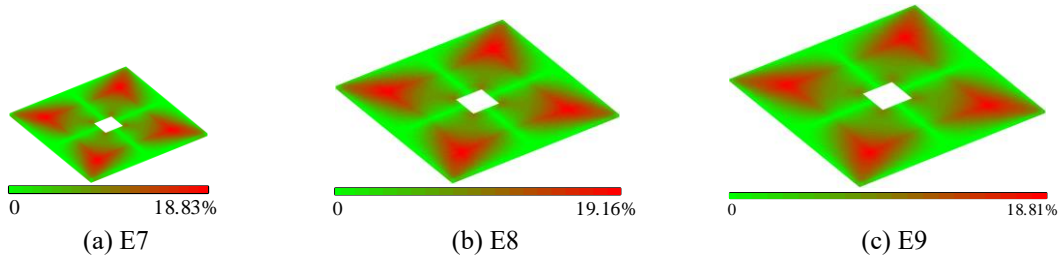


Fig. 16 Warping deformation proportion cloud diagrams of models E7 to E9

Table 7 Dimensional parameters of models E10 to E11

Serial number	Side length of plate /mm	Thickness/mm	Thickness-to-span ratio	Side length of hole /mm	Ratio of hole side length to plate side length	Number of elements used in two directions
E10	300	5	1:60	100	1:3	60×60
E11	360	5	1:72	120	1:3	72×72

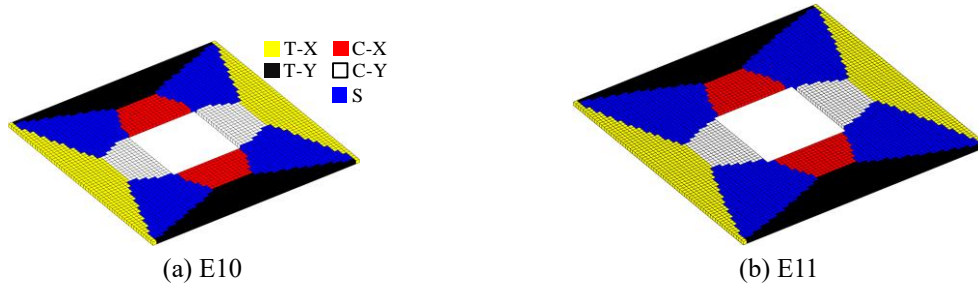


Fig. 17 Deformation decomposition diagrams of models E10 to E11

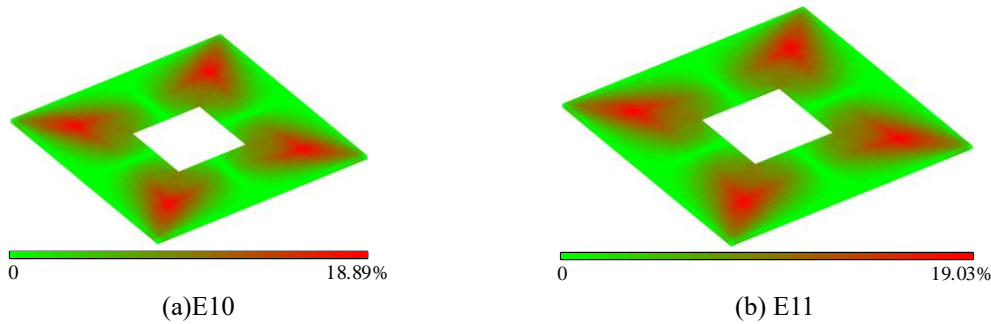


Fig. 18 Warping deformation proportion cloud diagrams of models E10 to E11

corners and adjacent positions of the hole.

For thin plates E10 and E11, the ratio of the side length of the hole to the side length of the plate is further increased to 1:3, as shown in Table 7. The deformation decomposition is carried out, and the deformation decomposition diagrams are shown in Figs. 17 to 18.

By comparing Fig. 15 and Fig. 17, it can be seen that when the ratio of the side length of the hole to the side

length of the plate is greater than 1:3, the area dominated by shear deformation begins to expand from the corners of the hole to both sides. Therefore, the ratio of the side length of the hole to the side length of the plate should not be greater than 1:3. The 1/3 of the side length of the plate should be taken as the upper limit of the side length of the hole. In addition, Fig. 18 shows that when the ratio of the side length of the hole to the side length of the plate is 1:3, the

warping deformation is still not negligible.

5. Conclusions

Based on the orthogonality and mechanical balance, the deformation basis matrix of the four-node square thin plate element is constructed. Using the deformation basis matrix, the comprehensive deformation of the element can be decomposed into completely orthogonal basic deformations, and then applied to the finite element analysis of the thin plate structures. The correctness of the proposed deformation decomposition method is verified by comparison with the finite element strain results.

Compared with the traditional finite element strain analysis, which can only solve the nodal displacement and strain value of the element, the basic deformation information of the four-node square thin plate element can be directly obtained based on the deformation decomposition method. Under the action of uniformly distributed load, the warping deformation cannot be ignored at the corners of the thin plate. The following conclusions can be drawn from the deformation decomposition of the four-side-fixed plate with a hole in the center:

- With the increase of the hole size, the proportion of warping deformation is increasing at the corners of the central hole. In addition, the areas dominated by shear deformation begin to appear at the corners of the central hole. Therefore, warping deformation resistance design and shear deformation resistance design should be considered.
- When the ratio of the side length of the hole to the side length of the thin plate is 1:6, the main area of shear deformation at the corner of the hole and the main area of shear deformation at the corner of the thin plate begin to be connected. The shear deformation resistance design and the warping deformation resistance design should be added along the connecting lines.
- When the ratio of the side length of the hole to the side length of the plate is greater than 1:3, the area dominated by shear deformation begins to expand from the corners of the hole to both sides. 1/3 of the side length of the plate should be taken as the upper limit of the side length of the hole. At this time, the warping deformation is still not negligible.

Acknowledgments

This work was supported by the National Natural Science Foundation of China (Grant No. 51878621), the Natural Science Foundation of Henan Province (Grant No. 222300420316), the China Postdoctoral Science Foundation (Grant No. 2022M712905) and the Key Research Project of Henan Higher Education Institutions (Grant No. 22A560005).

References

ACI 318 (2011), Building Code Requirements for Structural

- Concrete and Commentary, American Concrete Institute, Farmington Hills, MI, USA.
- Ali, N., Calaf, M. and Cal, R.B. (2021), "Cluster-based probabilistic structure dynamical model of wind turbine wake", *J. Turbul.*, **22**(8), 497-516. <https://doi.org/10.1080/14685248.2021.1925125>.
- Dehghani, A., Hayatdavoodi, A. and Aslani, F. (2021), "The ultimate shear capacity of longitudinally stiffened steel-concrete composite plate girders", *J. Constr. Steel Res.*, **179**(9), 106550. <https://doi.org/10.1016/j.jcsr.2021.106550>.
- Gere, J.M. and Timoshenko, S.P. (1997), *Mechanics of Materials*, Van Nostrand Reinhold Co., New York, NY, USA.
- Girfoglio, M., Quaini, A. and Rozza, G. (2021), "A POD-Galerkin reduced order model for a LES filtering approach", *J. Comput. Phys.*, **436**, 110260. <https://doi.org/10.1016/j.jcp.2021.110260>.
- Hassani, S. (2013), *Mathematical Physics: A Modern Introduction to its Foundations*, 2nd Edition, Springer International Publishing, New York, NY, USA.
- Hwang, H., Ma, G. and Kim, C. (2019), "Minimum thickness of flat plates considering construction load effect", *Struct. Eng. Mech.*, **69**(1), 1-10. <https://doi.org/10.12989/sem.2019.69.1.001>.
- Jafari, M. and Ardalani, E. (2016), "Stress concentration in finite metallic plates with regular holes", *Int. J. Mech. Sci.*, **106**, 220-230. <https://doi.org/10.1016/j.ijmeecsci.2015.12.022>.
- Janiga, G. (2019), "Novel feature-based visualization of the unsteady blood flow in intracranial aneurysms with the help of proper orthogonal decomposition (POD)", *Comput. Med. Imag. Graph.*, **73**, 30-38. <https://doi.org/10.1016/j.compmedimag.2019.01.001>.
- Kalaycioglu, B., Alshaya, A. and Rowlands, R. (2019), "Experimental stress analysis of an arbitrary geometry containing irregularly shaped hole", *Strain.*, **55**(3), e12306. <https://doi.org/10.1111/str.12306>.
- Katili, I., Batoz, J., Maknun, I.J., Hamdouni, A. and Millet, O. (2015), "The development of DKMQ plate bending element for thick to thin shell analysis based on the Naghdi/Reissner/Mindlin shell theory", *Finite Elem. Anal. Des.*, **100**, 12-27. <https://doi.org/10.1016/j.finel.2015.02.005>.
- Kordolemis, A. and Weaver, P.M. (2017), "Geometric-material analogy for multiscale modelling of twisted plates", *Int. J. Solid. Struct.*, **110**, 24-35. <https://doi.org/10.1016/j.ijsolstr.2017.02.006>.
- Landau, L.D. and Lifshitz, E.M. (2009), *Theory of Elasticity*, 3rd Edition, World Book Inc, Beijing, BJ, CN.
- Lederle, R.E. and Hiller, J.E. (2012), "New warping and differential drying shrinkage models for jointed plain concrete pavements derived with nonlinear shrinkage distribution", *Transp. Res. Rec.*, **2305**(1), 3-13. <https://doi.org/10.3141/2305-01>.
- Li, H., Yi, N., Li, Z., Xu, Z. and Han, Q. (2020), "Modeling of amplitude-dependent damping characteristics of fiber reinforced composite thin plate", *Appl. Math. Model.*, **80**, 394-407. <https://doi.org/10.1016/j.apm.2019.11.048>.
- Loredo, A. (2016), "A multilayered plate theory with transverse shear and normal warping functions", *Compos. Struct.*, **156**, 361-374. <https://doi.org/10.1016/j.compstruct.2015.08.084>.
- Piana, G., Lofrano, E., Carpinteri, A. and Ruta, G. (2021), "Effect of local stiffeners and warping constraints on the buckling of symmetric open thin-walled beams with high warping stiffness", *Meccanica*, **56**(8), 2083-2102. <https://doi.org/10.1007/s11012-021-01349-9>.
- Piltner, R. (1992), "A quadrilateral hybrid-Trefftz plate bending element for the inclusion of warping based on a three-dimensional plate formulation", *Int. J. Numer. Meth. Eng.*, **33**(2), 387-408. <https://doi.org/10.1002/nme.1620330210>.
- Polizzotto, C. (2018), "A class of shear deformable isotropic elastic plates with parametrically variable warping shapes", *PMM-J. Appl. Math. Mech./Zeitschrift für Angewandte*

- Mathematik und Mechanik*, **98**(2), 195-221.
<https://doi.org/10.1002/zamm.201700070>.
- Ren, Y. and Wang, B. (2019), "L-shaped plate model for the analysis of the warping deformation of perforated diaphragms in box girder", *Thin Wall. Struct.*, **143**(SI), 106249.
<https://doi.org/10.1016/j.tws.2019.106249>.
- Saliba, N.G. and Gardner, L. (2018), "Deformation-based design of stainless steel cross-sections in shear", *Thin Wall. Struct.*, **123**, 324-332. <https://doi.org/10.1016/j.tws.2017.11.035>.
- Shang, Y., Cen, S. and Li, C. (2016), "A 4-node quadrilateral flat shell element formulated by the shape-free HDF plate and HSF membrane elements", *Eng. Comput.*, **33**(3), 713-741.
<https://doi.org/10.1108/EC-04-2015-0102>.
- Tang, S., Djenidi, L., Antonia, R. and Zhou, Y. (2015), "Comparison between velocity- and vorticity-based POD methods in a turbulent wake", *Exp. Fluid.*, **56**(8), 169.
<https://doi.org/10.1007/s00348-015-2038-z>.
- Taylor, G.I. (1933), "The buckling load for a rectangular plate with four clamped edges", *PMM-J. Appl. Math. Mech./Zeitschrift für Angewandte Mathematik und Mechanik*, **13**(2), 1521-4001.
<https://doi.org/10.1002/zamm.19330130222>.
- Tuna, M. and Trovalusci, P. (2020), "Stress distribution around an elliptic hole in a plate with 'implicit' and 'explicit' non-local models", *Compos. Struct.*, **266**, 113843.
<https://doi.org/10.1016/j.compstruct.2021.113843>.
- Wang, F., Zheng, Y. and Chen, C. (2018), "Nonlinear bending of rectangular magneto-electroelastic thin plates with linearly varying thickness", *Int. J. Nonlin. Sci. Numer.*, **19**(3-4), 351-356. <https://doi.org/10.1515/ijnsns-2015-0105>.
- Wang, W. and Spencer, B.J. (2021), "Numerical solution for the stress near a hole with corners in an infinite plate under biaxial loading", *J. Eng. Math.*, **127**(1), 1-25.
<https://doi.org/10.1007/s10665-021-10104-8>.
- Xu, L., Li, W., Wang, X., Wan, M. and Jiang, M. (2017), "Plastic deformation behavior in laser bending of elastic pre-loaded metal plate", *Int. J. Adv. Manuf. Tech.*, **90**(9-12), 3397-3406.
<https://doi.org/10.1007/s00170-016-9643-8>.
- Yan, X.Q. (2006), "Cracks emanating from circular hole or square hole in rectangular plate in tension", *Eng. Fract. Mech.*, **73**(12), 1743-1754. <https://doi.org/10.1016/j.engfracmech.2006.02.003>.
- Zhu, Y., Mao, K. and Yu, X. (2020), "A general model for prediction of deformation from initial residual stress", *Int. J. Adv. Manuf. Tech.*, **109**(3-4), 1093-1101.
<https://doi.org/10.1007/s00170-020-05683-2>.